Monatshefte für Chemie (2002)
DOI 10.1007/s00706-002-0509-4

Monatshefte für Chemie
Chemical Monthly
Printed in Austria

Potential and Limitations of 2D ^{1}H–^{1}H Spin-Exchange CRAMPS Experiments to Characterize Structures of Organic Solids

Jiri Brus[1,*], **Hana Petříčková**[2], and **Jiri Dybal**[1]

[1] Institute of Macromolecular Chemistry, Academy of Sciences of the Czech Republic, Heyrovsky Sq. 2, CZ-162 06 Prague 6, Czech Republic
[2] Institute of Chemical Technology, CZ-Prague, Technicka 5, 166 28 Prague 6, Czech Republic

Received May 28, 2002; accepted (revised) July 1, 2002
Published online November 7, 2002

Summary. A brief overview of our recent results concerning the application of 2D CRAMPS experiments to investigate a wide range of materials is presented. The abilities of the 2D ^{1}H–^{1}H spin-exchange technique to characterize the structure of organic solids as well as the limitations resulting from segmental mobility and from undesired coherence transfer are discussed. Basic principles of ^{1}H NMR line-narrowing and procedures for analysis of the spin-exchange process are introduced. We focused to the qualitative and quantitative analysis of complex spin-exchange process leading to the determination of domain sizes and morphology in heterogeneous multicomponent systems as well as the characterization of clustering of surface hydroxyl groups in polysiloxane networks. Particular attention is devoted to the determination of the ^{1}H–^{1}H interatomic distances in the presence of local molecular motion. Finally we discuss limitations of the ^{13}C–^{13}C correlation mediated by ^{1}H–^{1}H spin exchange to obtain structural constraints. The application of *Lee-Goldburg* cross-polarization to suppress undesired coherence transfer is proposed.

Keywords. CRAMPS; 2D solid-state NMR; *Lee-Goldburg*; Miscibility of polymers; Clustering of surface silanols; Molecular dynamics.

Introduction

The importance of NMR follows from its unique selectivity differentiating various chemically distinct sites on the basis of their chemical shifts. In solution-state NMR the protons are most important due to a nearly 100% natural abundance and the highest gyromagnetic ratio γ. From this follows the best sensitivity of

* Corresponding author. E-mail: brus@imc.cas.cz

all naturally occurring nuclei. On the other hand, just this combination of properties dramatically complicates recording of ^{1}H NMR spectra in the solid state. Missing isotropic tumbling leads to a severe broadening of the NMR signals as a result of non-averaged anisotropic interactions. The dominant anisotropic interaction in solid-state ^{1}H NMR is dipolar coupling hindering resolution of chemically different sites. That is why one broad signal with a line-width of several tens of kHz is usually observed. The lack of ^{1}H NMR spectrum resolution does not mean the absence of structure information in the obtained spectra, it rather reflects its overcrowding in such an extent that we are not able to read out and understand it. Due to this fact various techniques have been proposed to increase the spectral resolution of ^{1}H NMR spectra because they provide valuable indications about the local chemical environment and a wide range of structural information.

In recent years we have investigated several systems by solid-state ^{1}H NMR spectroscopy. In the first part of this contribution we briefly summarize the basic concept of techniques leading to the averaging of anisotropic nuclear interactions and we introduce description and analysis of the spin-exchange process. In the second part we present our recent results concerning applications of two-dimensional (2D) ^{1}H spin-exchange experiments applied to the characterization of the structure and geometry of a wide range of materials. At first qualitative and quantitative data providing information about miscibility, morphology and domain sizes are discussed. Further, the investigation of clustering of surface hydroxyl groups including silanols and adsorbed water molecules in polysiloxane networks is introduced. Particular attention is paid to the precise measurement of ^{1}H–^{1}H interatomic distances in crystalline organic solids in the presence of local molecular motion. Finally we discuss the application of ^{13}C–^{13}C correlation mediated by ^{1}H–^{1}H spin exchange to obtain precise data leading to the extraction of ^{1}H–^{1}H spatial separation. The advantage of *Lee-Goldburg* irradiation to suppress undesired coherence transfer during cross-polarization steps is introduced.

Methods and Principles

Magic Angle Spinning (MAS)

One possible way how to compensate missing molecular motion is mechanical uniaxial rotation. It is known that anisotropic interactions such as dipolar coupling between a pair of nuclei or chemical shift anisotropy (CSA) have an orientation dependence that can be described by the second rank tensor [1, 2]. In such case physical rotation of the sample around the axis, which is inclined at the angle 54.7° (magic angle) with respect to static magnetic field leads to an averaging of anisotropy broadening to zero [3, 4]. If anisotropic interaction is refocused at the end of each rotor period (*i.e.* CSA) the originally broad static NMR signal is easily broken up into a sharp central signal reflecting isotropic chemical shift and series of spinning sidebands separated by the roation frequency ν_r. The line-widths of these signals are independent of the spinning speed (see Fig. 1A).

However, in the case of a multibody strongly dipolar-coupled spin-system the situation is quite different. In contrast to the previous case of CSA the line-widths of all ^{1}H signals are ν_r frequency dependent and the central signal and spinning

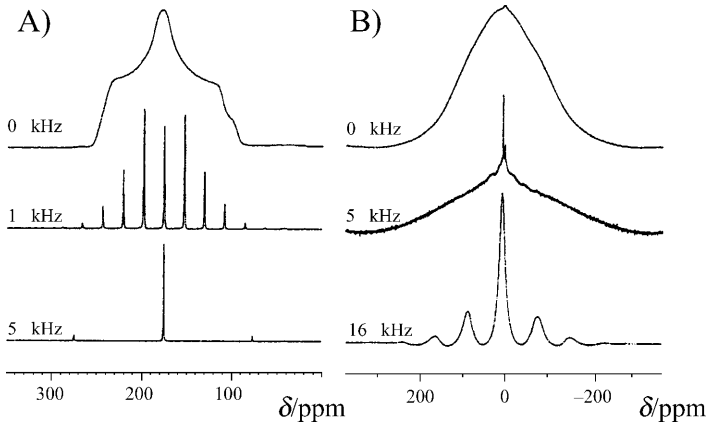

Fig. 1. ^{13}C NMR (A) and ^{1}H NMR (B) spectra of ^{13}C selectively labeled (C=O) glycine measured at various MAS spinning frequencies

side bands are still relatively broad. Even at moderately fast spinning speeds the ^{1}H NMR signals remain much larger than those observed in ^{13}C MAS NMR spectra. From Fig. 1B it is clear that a spinning speed of *ca.* 15 kHz, which is achieved with a standard 4-mm probe-head, is still not sufficient to provide reasonable good resolution. Recent development of new 2.5-mm probe-heads has made it possible to routinely achieve much greater rotation frequencies up to 35 kHz and even a rotation frequency of 50 kHz has been reported [5]. Such fast MAS leads to relatively well resolved spectra. However, the resolution of ^{1}H MAS NMR spectra still is not comparable with the resolution of spectra obtained for liquid samples and in addition ultra-high spinning speed induced substantial friction heating of the sample [6–8]. Temperature increase within the sample due to fast rotation may make-up to about 60 K, and temperature gradients within the samples (up to 17 K) may cause an additional broadening of signals [9]. That is why alternative procedures of narrowing ^{1}H signals in the solid state should be used in particular cases.

Multipulse ^{1}H Homodecoupling (Combined Rotation and Multiple-Pulse Spectroscopy)

The first classical multiple-pulse homodecoupling technique (WHH-4) was designed in 1968 [10]. It consists of many cycles, each made up of two solid-echo pulse pairs: that is, four 90° pulses are separated by windows of duration τ or 2τ (see Fig. 2A). As we would like to avoid a quantum mechanical treatment, we use only highly simplistic and intuitive description of the techniques. For more detailed analysis see *e.g.* [11–13]. In the analysis of these techniques, the duration of the pulses is assumed to be negligible. After a cycle of 6τ (for sufficiently short pulse-spacing τ) the spins effectively evolve under the average Hamiltonian reflecting only chemical shift and resonance offset. Stroboscopic detection at these times ($t = 6\tau$, in Fig. 2 asterisks indicate acquisition of one data point) therefore produces a time signal that is modulated only by chemical shift, resonance offset and heteronuclear dipole couplings. During the multiple-pulse sequence the precession no longer occurs around the direction of the static magnetic field; instead, the

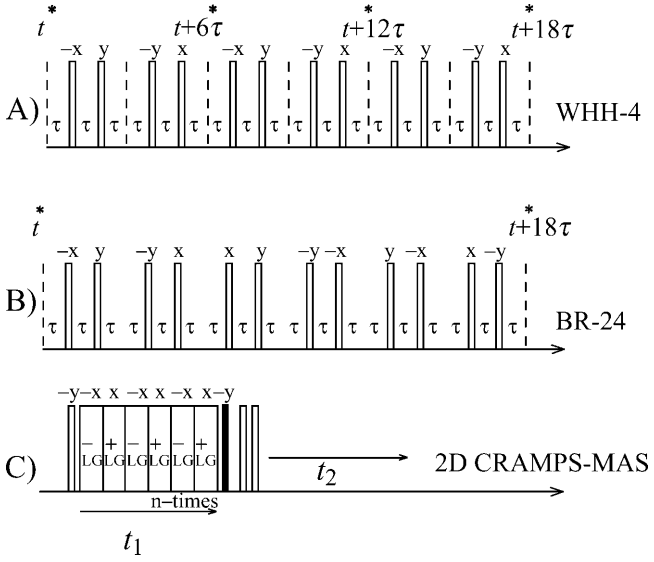

Fig. 2. Pulse schemes of homodecoupling sequences: (A) WHH4; (B) BR-24 (one half of the sequence) and (C) 2D CRAMPS-MAS experiment exploiting *Lee-Goldburg* decoupling during t_1 detection (the black block corresponds to the 54° pulse)

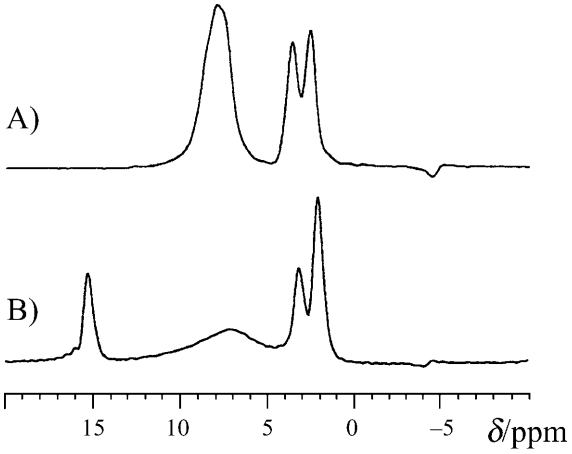

Fig. 3. ^{1}H CRAMPS spectra of glycine (A) and aspartic acid (B) measured by the BR-24 pulse sequence ($\pi/2$ ^{1}H pulse – 1.8 μs, small and large window 3.8 and 1.0 μs, MAS 2 kHz)

first-order average Hamiltonian causes a precession with an effective frequency $\omega^j_{\text{eff}} = \omega^j/\sqrt{3}$ around the effective-field unit vector $(1/\sqrt{3})(1,1,1)$. The ratio $\omega^j_{\text{eff}}/\omega^j$ is generally known as the frequency scaling factor. The applied train of *rf* pulses causes the rotation in spin space [10, 11] and dipolar broadening is suppressed. Well resolved ^{1}H MAS NMR spectra are achieved by simultaneous application of MAS refocusing chemical shift anisotropy [14–16] (see Fig. 3). This combination is termed as ''combined rotation and multiple-pulse spectroscopy'' (CRAMPS).

Several preconditions and approximations in the derivation of action of these pulse sequences indicate the special requirements for the use of multipulse

techniques: pulses with accurate flip angles and relative phases are needed. Also the pulse length and the spacing τ must be as small as possible. To reduce effects of pulse imperfection and higher-order terms of dipolar couplings, other pulse sequences based on WHH-4 have been developed. Among the various techniques, the MREV-8 sequence (*Mansfield-Rhim-Elleman-Vaughan*; consisting of two phase-cycled WHH-4) [17] seems to be highly robust. Further improvement provides technique BR-24 developed by *Burum* and *Rhim* [18] consisting of three partly nested MREV-8 cycles, which averages out the homonuclear interaction up to the third order (see Fig. 2B). Therefore this sequence provides best results in a well tuned spectrometer.

As mentioned above, sufficiently fast MAS considerably reduces dipolar broadening. From this fact one would expect that a multipulse sequence could be performed more easily at a high spinning speed leading to much more resolved spectra. However, both averaging techniques mutually interfere [19], which causes a rather dramatic loss of spectral resolution when a multipulse sequence is simply applied at high speed MAS conditions [20]. In fact, a spinning frequency less than 3 kHz is usually used. Under this condition (quasi-static limit) the sample is considered to be static during each cycle of the multipulse sequence. The mutual interference can be reduced by synchronization of the multiple-pulse sequence with MAS (variants of WHH-4 sequence were applied at moderately fast MAS, 10–15 kHz) [20–22]. Under such conditions the original philosophy of CRAMPS experiments is shifted. At fast MAS multipulse sequence may not completely remove dipolar broadening as required in quasi-static limit; rather, it is sufficient if the given sequence reduces dipolar couplings to such an extent that fast MAS can remove the residual contribution. Such experimental techniques are known as ''multiple-pulse assisted MAS''.

An alternative approach leading to averaging of homonuclear dipolar couplings is based on the *Lee-Goldburg* experiment [23], in which the offset of ^{1}H *rf* irradiation is set equal to $\omega_1/\sqrt{2}$, where ω_1 is the nutation frequency of the ^{1}H pulse ($|\omega_1| = |\gamma B_1|$). Using the vector model, the ^{1}H spins rotate under this irradiation around an effective field inclined at the angle 54.7° with respect to the static magnetic field. A significant enhancement of this technique was achieved by the frequency-switched modification of the *Lee-Goldburg* experiment (FSLG) [24, 25]. Instead of continuous irradiation, a series of 2π ^{1}H pulses with an offset switched between two LG conditions $\mp\omega_1/\sqrt{2}$ accompanied by a phase shift of π is applied. This technique works well for spinning speeds ranging from 10 to 16 kHz [26]. An alternative interpretation of the *Lee-Goldburg* technique was recently presented by *Vinogradov* and co-workers [28]. In this experiment (phase-modulated *Lee-Goldburg* – PMLG) only the phase of a series of adjacent pulses is changed. The frequency of the B_1 field remains constant. It was shown that the zero-order term of the average Hamiltonian vanishes when the modulation of the pulse phase $\phi(t) = \omega_{\mathrm{PMLG}} t$ statisfies the condition: $|\omega_{\mathrm{PMLG}}| = \omega_1/\sqrt{2}$ and the duration of the LG irradiation unit corresponds to a 2π rotation of the proton magnetization about the effective field, *i.e.* $t_{\mathrm{LG}} = \sqrt{(2/3)}(2\pi/\omega_1)$. From this it is evident that the angle through which *rf* precesses in one LG unit is given by $\alpha_{\mathrm{LG}} = |\omega_{\mathrm{PMLG}}| t_{\mathrm{LG}} = 207.8°$. As symmetrization is required to ensure the removal of odd-order terms in the dipolar Hamiltonian, the sign of the phase modulation has to be negated between

alternate LG units. Hence, during the first part of the PMLG sequence, the *rf* field precesses from 0° to 208° and then to 180°, after a 180° flip, during the second half of the PMLG unit. This constitutes a unit of PMLG which is executed by a series of short pulses with well-defined phases, α_i, for the *i*-th pulse. The duration of each pulse has been chosen to be *ca.* 1 μs and *rf* field strength 82 kHz. These originally developed pulse sequences applying both concepts of *Lee-Goldburg* irradiation (FSLG and PMLG) have no windows for direct signal detection; that is why ^{1}H NMR spectra are obtained using an indirect detection scheme (see Fig. 2C). The resolution of the obtained spectra (t_1 projection of the 2D experiments) is very promising. For instance, the halfwidth of ^{1}H NMR signals of malonic acid is 0.3 ppm [28]. Recently, a wide range of two-dimensional (2D) and three-dimensional (3D) experiments has been designed on the basis of these homodecoupling schemes [26–30]. Quite recently, successful insertion of detection windows in the PMLG schemes has been reported [31]. It has to be noted that the first attempt in this direction was made by *Levitt et al.* [32] by inserting windows in the FSLG sequence. By this way high-resolution ^{1}H NMR spectra can be measured in a 1D fashion. Application of windowed PMLG simplifies ^{1}H–^{1}H correlation experiments for signal assignment and distance measurements and enables an inverse detection to enhance the sensitivity to experiments.

^{1}H–^{1}H Spin Exchange (Spin Diffusion)

Although the strong spin interaction (given by the combination of nearly 100% natural abundance of ^{1}H nuclei and the highest gyromagnetic ratio γ) highly complicates the recording of ^{1}H NMR spectra for the solid state, it offers interesting structural information. For instance, it can be provided by the spatial transfer of z magnetization between dipolar-coupled spins. Such a transfer is termed ''spin exchange'' or ''spin diffusion'' [33] and it is most efficient between protons. The quantum mechanical treatment of spin exchange between two spins revealed its oscillatory behavior. However, for systems of many spins the complicated network of couplings cancels all oscillations thus leading effectively to diffusive behavior [2].

It has to be stressed that ^{1}H spin diffusion in the solid-state is a coherent, fully reversible process [34] in contrast to relayed ^{1}H polarization transfer based on the multistep nuclear *Overhauser* effect (N*O*E) observed in certain solution-state NMR experiments, which is also termed spin diffusion. The latter process is an incoherent cross-relaxation induced by the stochastic modulation of local fields by molecular motion. Due to its stochastic time dependence this process cannot be refocused.

Spin-diffusion experiments are typical exchange experiments, consisting of an evolution or selection period, a mixing time t_m, and a detection period. The time dependence of the spin-diffusion process contains information on the domain size in heterogeneous materials: in systems with small domains, the magnetization equilibrates faster than in a system consisting of large particles. Generally, spin diffusion typically probes the smallest distances since the equilibrium occurs *via* the shortest path. For spin diffusion to occur, a spatially inhomogeneous z magnetization distribution has to be generated. The magnetization of one component is selected while the magnetization of the second component is suppressed. During a

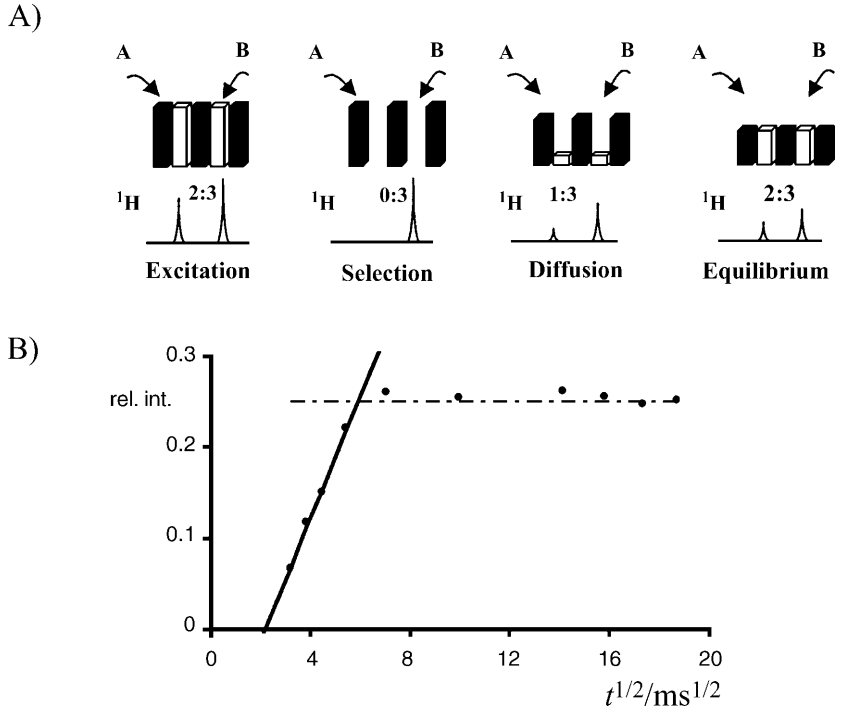

Fig. 4. (A) Basic scheme of the spin-diffusion experiment: Magnetization of the A component is selected during the selection period to generate the magnetization gradient. During mixing time t_m spin-diffusion occurs, which is detected by an increase of the signal intensity of the B component. (B) Spin-exchange built-up data

mixing period, magnetization of the selected component is transferred by double and zero-quantum transitions to neighboring spins. At short mixing times, ^{1}H polarization is transferred between the nearest spins, while at longer times, relayed polarization transfer to further spins occurs at a rate proportional to $1/r_{ij}^3$. Then, the distribution of magnetization of one component is monitored in the NMR spectrum (see Fig. 4). Thus, ^{1}H–^{1}H spin-exchange experiments can be used to measure short-range distances providing constraints for structure determination and signal assignment using detection of spin-exchange process at very short mixing times, while relayed ^{1}H–^{1}H spin exchange (spin diffusion) makes it possible to study long-range ordered structures on a 0.5–200 nm scale.

Analysis of Spin-Exchange Built Up-Curves

In order to obtain information about the domain size from spin-exchange data, a simulation of the time-dependence of polarization exchange has to be performed. In general, the rate of magnetization exchange $P(t)$ between two nuclei j and k is given by Eq. (1)

$$P(t) = \tfrac{1}{2}\pi g_0^{jk}(\omega_j - \omega_k)\omega_D^2 t \tag{1}$$

where the term $g_0^{jk}(\omega_j - \omega_k)$ is proportional to the overlap between the j-th and k-th ^{1}H NMR signals, while ω_D measures the dipolar coupling between the two nuclei

[35]. In a strongly dipolar-coupled multibody spin-system, however, the phenomenological description based on *Fick*'s second law is usually used. Up to now, several approaches and procedures to extract the desired information have been proposed: a general initial-rate approximation, a rigorous solution for lamellar structures, related approximation for more complicated disordered morphologies, and a versatile lattice-calculation approach for arbitrary distributions of diffusivity values and initial z magnetization [2, 36–39]. In the simplest initial-rate approximation, analyzing the straight-line part of the spin-exchange built-up curve, the displacement of polarization between two neighbouring spins can be described by relation (2)

$$r = \left(\frac{4}{3} D t_m\right)^{1/2} \tag{2}$$

proposed by *Van der Hart et al.* [40], which is a special case of a generally derived spin-diffusion equation for two-component systems [2, 41, 42]:

$$d_{\mathrm{A}} = 2\frac{\varepsilon}{f_{\mathrm{B}}}\left(\frac{1}{\pi} D t_m^s\right)^{1/2} \tag{3}$$

d_{A} is the size of A component, f_{B} the volume fraction of B component, t_m^s the time of the straight line intersection with the $I = 100\%$ (*i.e.* $I = I_{\mathrm{B}}$ ($t_m \to \infty$)) and ε is the dimensionality of the spin-exchange process (*i.e.* the number of orthogonal directions relevant for the magnetization transfer). From the dimensionality ε, one can estimate the morphology of the studied system (lamellar – $\varepsilon = 1$; cylindrical – $\varepsilon = 2$; spherical – $\varepsilon = 3$). However, a recent study [37] has indicated that the determination of the morphology of an unknown system is very rough, because all models are based on assumptions which are not quite realistic (*e.g.*, regular repetition of the domains, the same shape of the domains, and Gaussian distribution of their size, etc.). The crucial parameter for accurate analysis is the spin-diffusion (spin-exchange) coefficient D reflecting the strength of ^{1}H–^{1}H dipolar interactions within each component. For the analysis of clearly motionally heterogeneous two-component systems, the knowledge of the diffusivity of both components is required. If the diffusivities of the components differ ($D_{\mathrm{A}} \neq D_{\mathrm{B}}$), an effective spin diffusion D_{eff} coefficient has to be used.

$$\sqrt{D_{\mathrm{eff}}} = \frac{2\sqrt{D_{\mathrm{A}} D_{\mathrm{B}}}}{\sqrt{D_{\mathrm{A}}} + \sqrt{D_{\mathrm{B}}}} \tag{4}$$

The exact diffusivity D was determined from spin-diffusion built-up curves only for a well-defined material with known morphology and domain size, such as the diblock copolymer *PS-PMMA* (polystyrene-polymethylmethacrylate) the structure of which as been investigated by small-angle X-ray scattering and transmission electron microscopy [36]. The obtained value $D = 0.8 \pm 0.2\,\mathrm{nm^2\,ms^{-1}}$ is generally used for highly rigid organic solids. However, for systems with unknown geometry other approaches have to be used. In general, the diffusivity is expressed in terms of local dipolar fields proposed by *Cheung* [43, 44]. For instance, the following Eqs. (5) and (6), relating D with the ^{1}H line-width at half intensity

$\Delta\nu_{1/2}$ were proposed for the Gaussian line-shape reflecting the rigid component [38, 45].

$$D_{\text{rig}} = \frac{1}{12}\sqrt{\frac{\pi}{2\ln 2}}\langle r^2\rangle \Delta\nu_{1/2} \tag{5}$$

$$D_{\text{rig}} = \Delta\nu_{1/2}\frac{\langle r^2\rangle}{3} \tag{6}$$

Here $\langle r^2\rangle$ is the square average of the ^{1}H–^{1}H internuclear distance, which is assumed to be ranging in organic solids from 0.2 to 0.25 nm. For mobile components characterized by Lorentzian ^{1}H NMR line-shape, the diffusivity is expressed by Eq. (7), where α is the cutoff parameter.

$$D_{\text{mob}} = \frac{1}{6}\langle r^2\rangle[\alpha\Delta\nu_{1/2}]^{1/2} \tag{7}$$

Alternative expressions relating diffusivity to T_2 relaxation have been reported by *Mellinger et al.* [41]:

$$D_{\text{mob}} = 8.2\times10^{-6}T_2^{-1} + 0.007 \tag{8}$$

$$D_{\text{mob}} = 4.4\times10^{-5}T_2^{-1} + 0.26 \tag{9}$$

Relations (8) and (9) are supposed to be valid for regions corresponding to $0 < T_2^{-1} < 1000$ and $1000 < T_2^{-1} < 3500$ Hz.

For mobile amorphous poly(ethylene oxide) (*PEO*) with the ^{1}H NMR linewidth of *ca.* 0.6–1.7 kHz and amorphous polyethylene (*PE*) with the linewidth of *ca.* 1.8 kHz, diffusivities in the range of 0.09–0.15 $\text{nm}^2\,\text{ms}^{-1}$ have been reported [36, 46–48]. Lower values ranging from *ca.* 0.03 to 0.08 $\text{nm}^2\,\text{ms}^{-1}$ have been determined for mobile *PEO* and polyisoprene by *Mellinger et al.* [41]. *Spiegel et al.* [49] have found a diffusivity of 0.05 $\text{nm}^2\,\text{ms}^{-1}$ for polyisoprene. For soft polyurea segments [50] and highly mobile aliphatic side-chains [51] spin-diffusion coefficients have been determined to be 0.04 and 0.05 $\text{nm}^2\,\text{ms}^{-1}$. For a rubbery poly(epichlorohydrin)/poly(vinyl acetate) blend [52], even a value of 0.01 $\text{nm}^2\,\text{ms}^{-1}$ has been reported. Mobile poly(dimethylsiloxane) chains cross-linking polyimide chains have been characterized by $D = 0.09\,\text{nm}^2\,\text{ms}^{-1}$ [53]. A diffusivity of 0.4 $\text{nm}^2\,\text{ms}^{-1}$ has been determined [51] for the aromatic main-chain protons of hard segments of poly(1,4-phenyleneterephthalimide) and poly(1,4-phenylenepyromellitimide), as well as for an aromatic poly(ester-urethane) elastomer [43, 54]. For crystalline domains of *PEO*, spin-diffusion coefficients [46] are assumed to be 0.29–0.32 $\text{nm}^2\,\text{ms}^{-1}$. Much higher diffusivities have been reported for rigid crystalline solids and densely packed polymers; the diffusivity of *PE* [46, 47] is 0.7–0.8 $\text{nm}^2\,\text{ms}^{-1}$ and of crystalline alanine [55] it is 0.6–0.8 $\text{nm}^2\,\text{ms}^{-1}$.

Results and Discussion

Due to the relatively low resolution of ^{1}H NMR spectra of solids, one-dimensional (1D) spin-diffusion experiments have been predominantly used up to the recent past to study the homogeneity of various mixtures and the miscibility of their

components [36, 40, 56]. The application of such 1D experiments only for the investigation of relatively simple systems follows also from the necessity to create an initial magnetization gradient to provoke spin diffusion. This selection period is often based on T_2 or T_1 relaxation [57, 58] or multiple-pulse dipolar filters [50, 51, 58, 59], which discriminate components substantially differing in mobility. That is why spin diffusion has been predominantly studied only between two dynamically different components, although techniques based on chemical shift filtering [36, 58, 60] and selective saturation transfer [61, 62] have been also applied. A significant increase in resolution and generalization of spin-exchange experiments has been provided by two-dimensional (2D) technique proposed by *Caravatti et al.* [63] making it possible to observe polarization transfer between all sites resolved in a 2D ^{1}H–^{1}H CRAMPS correlation spectrum. If various protons in a magnetic field resonate at different energy levels the observation of spin exchange between these protons is permitted [35].

During the past two decades, a wide range of materials has been analyzed by this or similar 2D techniques [64–69]. A typical example of a semi-quantitative interpretation of 2D spin-exchange CRAMPS experiment can be demonstrated on the investigation of the extent of mixing of multicomponent polymer blends based on semicrystalline polycarbonate (*PC*) and semicrystalline *PEO* (*PC-PEO*) [48]. As displayed in Fig. 5, cross-peaks indicating proximity between aromatic and methyl protons of *PC* molecules are fully equilibrated after 250 μs. This indicates the shortest interatomic distance between methyl and aromatic protons within one monomer unit of *ca*. 0.3 nm, which is in accord with structural models of *PC*. The first cross-signals indicating dipolar interaction between methylene protons of *PEO* and both-type protons of the *PC* molecule are perceptible in a 2D spectrum measured with 500 μs mixing time. This indicates an intimate mixing of the amorphous phases of both components. However, even after 10 ms mixing time, the signals in the 2D spectrum are not yet completely equilibrated, which means that heterogeneities larger than several nanometers are present in this system. This heterogeneities correspond to crystallites of *PEO* and *PC*. These results reveal the complex morphology and arrangement of both polymer components.

Domain Size in the Diblock Copolymer PE-PEO

Detailed analysis of the spin-diffusion built-up curve demonstrates the power of this technique. The diblock copolymer *PE-PEO* provides an example of a system with relatively complicated morphology, because both polymer blocks are semicrystalline. Both chemically distinct $-CH_2-$ units are resolved in a 2D CRAMPS spectrum (see Fig. 6) allowing to obtain accurate spin-exchange data (see Fig. 7). From the known composition of the copolymer and taking into account the fraction of crystalline and amorphous phase, we estimated the effective spin diffusion coefficient $D_{\mathrm{eff}} = 0.4\,\mathrm{nm}^2\,\mathrm{ms}^{-1}$. In the first approximation, a simple two-component phase-separated system consisting of domains of *PE* and *PEO* was assumed. From the analysis of spin diffusion by this model (dashed line in Fig. 7) it was found that both components form domains with the average size *ca.* 6.5 nm in lamellar morphology ($\varepsilon = 1$). Consequently the long period is 13 nm. From the known number-average polymerization degree (X_n) 170 and 109 of *PE* and *PEO*

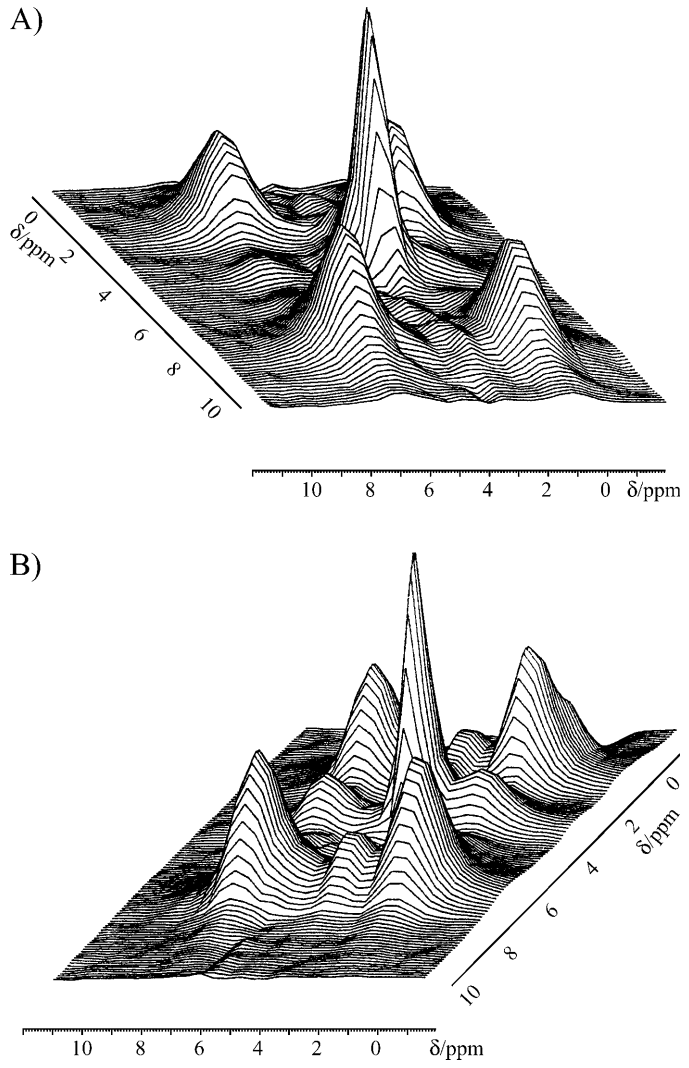

Fig. 5. 2D ^{1}H CRAMPS spectrum of the polymer blend *PC-PEO* measured with a 500 µs (A) and 10 ms mixing period (B)

chains it is clear that lamellae do not consist of extended chains, the theoretical lengths of which are 41 and 30 nm. This indicates extensive folding of both types of polymer chains. However, the model of a simple two-phase system does not quite fit the experimental dependence. That is why we modified the numerical simulation of the spin diffusion so that the single-spin-diffusion process was extended to a double-spin-diffusion process. The slow and fast spin-diffusion processes are superimposed and take place simultaneously. We propose that the first process apparent at the beginning of spin diffusion is a fast magnetization transfer between both components intimately mixed in the amorphous phase. For well-mixed polymer chains, cylindrical morphology and thus a dimensionality of $\varepsilon = 2$ is the best choice. The slow spin-diffusion process corresponds to the magnetization transfer involving substantially larger crystallites of both polymer chains. Simulation of spin exchange process according to this model revealed that

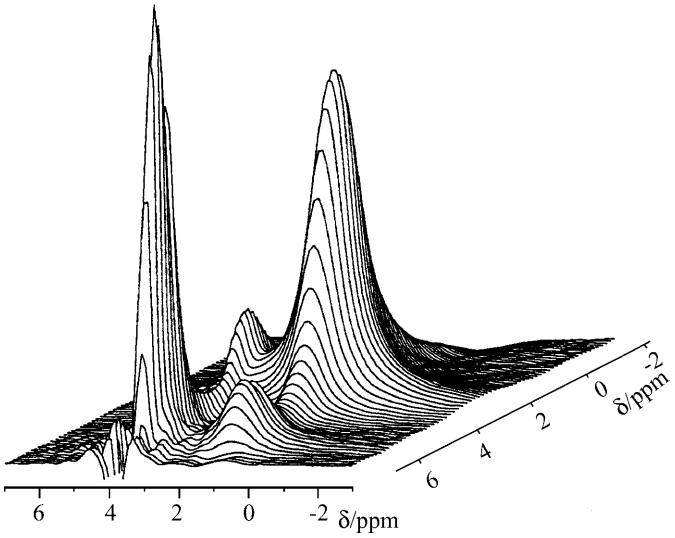

Fig. 6. 2D ^{1}H CRAMPS spectrum of the diblock copolymer *PE-PEO* measured with a 10 ms mixing period

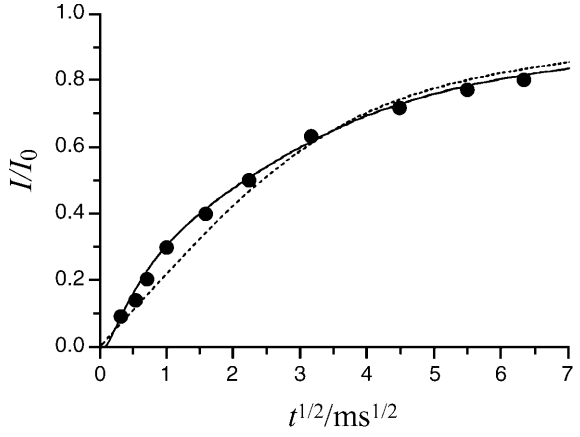

Fig. 7. Experimental (dots) and simulated (dashed and solid lines) spin-diffusion dependences of cross-peak intensity on mixing time obtained for the diblock copolymer *PE-PEO*

both components (*PE* and *PEO*) form relatively small domains with diameters *ca.* 1.0 and 0.5 nm in the amorphous phase, while crystallites are substantially larger, *ca.* 6.0 nm. The long period is *ca.* 13.5 nm, which exactly corresponds with the long period calculated for the simple model discussed above. This self-consistence of the obtained results proves the reliability of the applied model.

Clustering of Surface Hydroxyls in Siloxane Networks

Characterization of structure and geometry of organic polymer systems is not the only use of spin-exchange experiments. Recently, the simulation of a build-up curve has been used to investigate membrane peptide topology [70], as well as

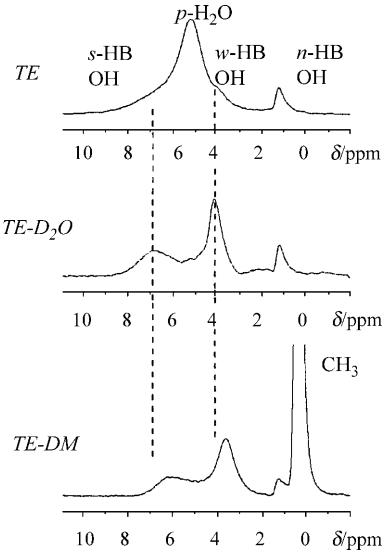

Fig. 8. ^{1}H CRAMPS NMR spectra of silica networks *TE*, *TE*-D_2O, and *TE-DM*

hydrogen-bonding and the size of clusters of various hydroxy groups in organically-modified polysiloxane networks [71].

Polysiloxane and polysilsesquioxane networks are short-range-ordered materials intermediate between the completely crystalline cristobalite and the least ordered silicate glasses [72–75]. Four basic types of hydroxyl groups have been detected in the CRAMPS spectrum even in hydrated silica gel (*TE*) prepared by polycondensation of tetraethoxysilane (see Fig. 8): strongly hydrogen-bonded (*s*-HB OH) and weakly hydrogen-bonded hydroxyl groups (*w*-HB OH), physisorbed water (*p*-H_2O) and non-hydrogen-bonded silanols (*n*-HB OH) at 7.0, 4.3, 5.2, and 1.4 ppm. Well-resolved signals in CRAMPS spectra of partially deuterated silica network (*TE*-D_2O) excludes fast chemical exchange between various hydroxyl sites and reflect a limited number of possible arrangements of strongly and weakly hydrogen-bonded OH. As the position of these ^{1}H NMR signals reflects the strength of hydrogen bonds it is clear that the network of hydrogen bonds is neither uniform nor random. Rather, both types of hydroxyl groups form several structures differing by the most probable length of hydrogen-bonds.

The presence of methyl substituents in the modified network prepared by co-condensation of tetraethoxysilane and dimethyldiethoxysilane (*TE-DM*) moves chemical shifts of signals of both strongly and weakly hydrogen-bonded hydroxyls toward higher field (see Fig. 8). Although this indicates a decrease in the hydrogen-bond strength, the replacement of silanol sites by methyls does not completely destroy the formation of hydrogen-bonding networks involving silanols and water molecules.

We have studied ^{1}H–^{1}H interatomic distances and the size of various OH clusters in detail [71]. Even though it is generally accepted that silanols reflected by the signal at 1.4 ppm are isolated and ''water-inaccessible'', the appearance of a cross-peak correlating it to the 5.2 ppm signal clearly proves spin exchange between these silanols and physisorbed water (see Fig. 9A). Their mutual distance is smaller

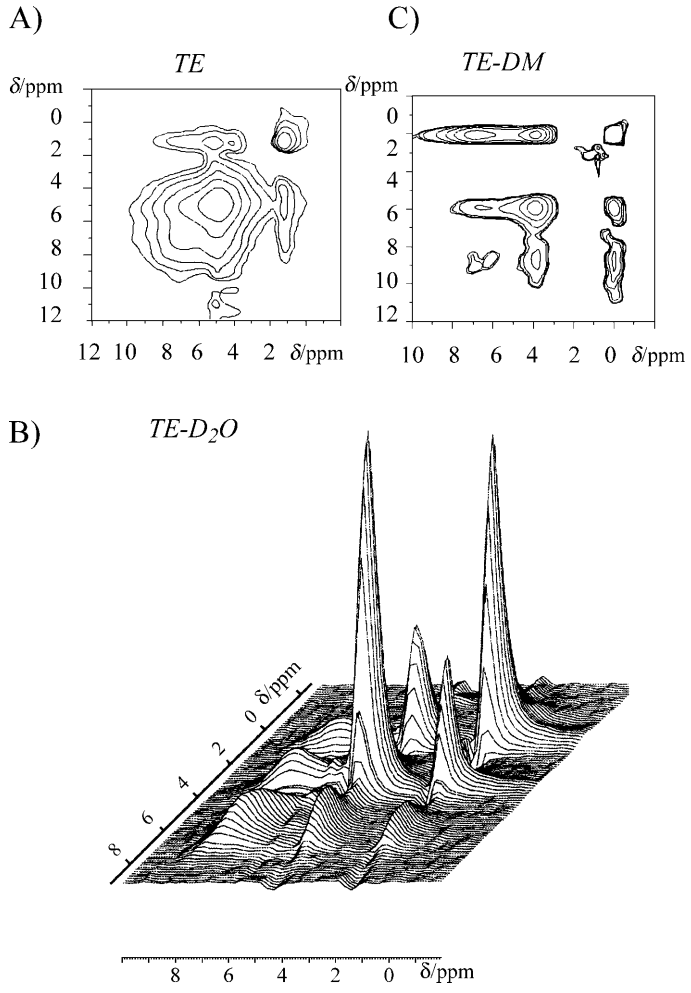

Fig. 9. 2D ^{1}H spin-exchange CRAMPS spectra of *TE*, *TE*-D_2O, and *TE-DM* systems measured at 20 ms spin-diffusion mixing time (A, B, and C)

than 0.4 nm. More detailed structure information was obtained for a partly deuterated sample (*TE*-D_2O). Quantitative data were derived from the simulation of spin-diffusion process for a two-component system with an interface with variable diffusivity and dimensionality ($\varepsilon = 1, 2, 3$). An effective spin diffusion coefficient was estimated according to *Assink*'s relation [76] from the ^{1}H T_2 relaxation constant. Basic parameters used for spin diffusion simulation are listed in Table 1.

The clusters of strongly and weakly hydrogen-bonded OH in the system *TE*-D_2O form relatively large regions and non-hydrogen-bonded silanols are dipolar-coupled with both types of these protons (see Fig. 9B). The absence of the interface following from the analysis of the spin-diffusion dependences (see Fig. 10A) indicates that all three types of OH are in mutual contact and the majority of strongly and weakly hydrogen bonded clusters are located at the surface. As the cross-peak intensity correlating strongly and weakly hydrogen-bonded OH does not tend to reach the theoretical equilibrium intensity, we suggest that a part of weakly hydrogen-bonded OH protons is quite isolated. From the best fits, employing our

Table 1. Transverse relaxation time, T_2, and calculated spin-diffusion coefficients, D

System	Hydroxyl type	T_2 ms	D[a] $mm^2\,ms^{-1}$
TE	*p*-H_2O	0.55	0.05
	s-HB OH	0.45	0.06
	w-HB OH	1.70	0.02
	n-HB OH	20.0	0.001
TE-DM	*s*-HB OH	0.60	0.05
	w-HB OH	1.80	0.02
	$-CH_3$	0.25	0.11

[a] Calculated by *Assink*'s method [76] $D_{\text{eff}} = 2(r_0)^2/T_2$, where r_0 is the *van der Waals* radius

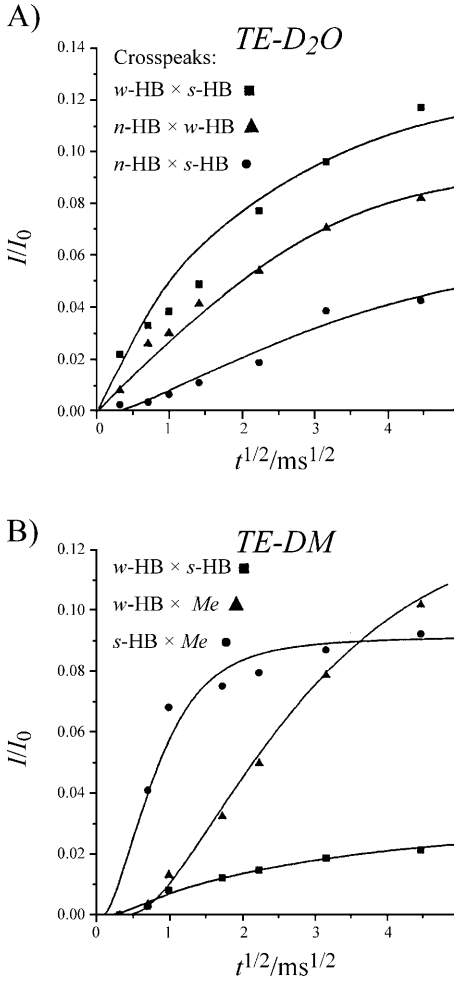

Fig. 10. Experimental (dots) and simulated (line) spin-diffusion curves: dependences of cross-peak intensity on mixing time

assumption about main dimensionality ($\varepsilon = 2$) we estimated the average size of hydroxyl clusters. Thus, it seems to be reasonable to conclude that weakly hydrogen-bonded OH groups form the largest clusters with a maximum diameter of about 1.5–2.0 nm, while clusters of strongly-hydrogen bonded OH are smaller with diameters below 1.0 nm. The smallest size was obtained for non-hydrogen-bonded silanols (*ca.* 0.5–0.4 nm) indicating that they can be formed by two geminal silanols and/or by two neighboring single silanols, which are in a geometry inappropriate to form a hydrogen bond.

The size of domains in a modified network *TE-DM* of strongly and weakly hydrogen-bonded OH groups is approximately the same as in the case of a net silica network. Methyl groups are in close contact with both types of clusters confirming that the presence of a small number of methyl units at the surface does not interrupt the hydrogen-bonding network. A high rate of equilibration of cross-peak intensity correlating methyls and strongly hydrogen-bonded OH (see Fig. 10B) reflects their intimate mixing. The calculated size of the dimethylsiloxane domains of about 1 nm indicates that the dimethylsiloxane monomer units occur in pairs. Significant interface was found between methyls and weakly hydrogen-bonded silanols. We propose that this interface reflects a portion of methyl groups which are surrounded only by strongly hydrogen-bonded OH.

Determination of ^1H–^1H Interatomic Distance

Significant progress has recently been made in the improvement in homonuclear dipolar decoupling sequences [27, 28, 77, 78]. Resolutions sufficient to distinguish signals having chemical shift differences as small as 0.5 ppm have been achieved. As ^{1}H NMR signals are usually detected indirectly, three-dimensional (3D) techniques [29, 30] have been used to measure ^{1}H–^{1}H correlations, although quite recent applications of windowed PMLG scheme has reduced the dimensionality of these experiments [31]. For instance, a 3D ^{1}H–^{1}H–^{13}C correlation experiment [30] correlated two high-resolution ^{1}H spectra with the ^{13}C NMR spectrum. Thereby the nearest ^{1}H–^{1}H interatomic distances can be selectively probed for each carbon resolved in the ^{13}C NMR spectrum. From this follows the possibility to measure ^{1}H–^{1}H correlations in solids providing structural constrains similar to those used to determine structures in liquid-state NMR.

On the basis of these facts, recently we have performed a detailed analysis of a spin-exchange process leading to the determination of the nearest ^{1}H–^{1}H interatomic distances [79]. We have found that difference in local molecular motions of various groups, even in virtually motionally homogeneous highly rigid systems (crystals of small organic molecules) substantially affect simulation of spin-exchange process. Our analysis of the spin-exchange process has been carried out on crystalline α-glycine, which is a highly suitable sample. The resulting ^{1}H CRAMPS spectrum is well resolved with a line-width of *ca*. 0.5–0.8 ppm and exhibits splittings of signal of α-protons reflecting their magnetic nonequivalence (different electrostatic potential charges [80]; see Fig. 11). Since fast rotation of NH_3^+ groups is assumed from the shape of the ^{1}H CRAMPS NMR signal reflecting a partial averaging of ^{14}N–^{1}H dipolar interactions [81, 82], NH_3^+ protons are considered to be a relatively mobile ^{1}H moieties, while a pair of α-protons is more rigid.

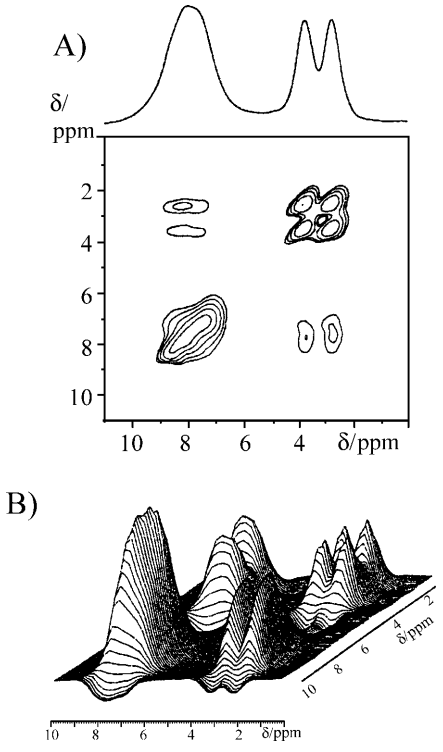

Fig. 11. 2D spin-exchange ^{1}H CRAMPS spectra measured at various mixing times, (A, 50 μs and B, 300 μs)

In practice it is impossible to detect this difference in molecular motion from a simple static ^{1}H NMR spectrum or a standard inversion recovery T_1 relaxation experiment, because fast ^{1}H spin flip-flop leads to a homogeneously broadened ^{1}H NMR spectrum (line-width *ca.* 50 kHz) and single-component relaxation behavior.

Evolution of cross-peak intensities as a function of $\sqrt{t_m}$ is displayed in Fig. 12. Analysis of the linear part of spin-exchange built-up curves was performed according to Eq. (3), which has been recently used [83] to calibrate spin-diffusion coefficients by analysis of intramonomer polarization transfers involving CH_3 and CH_2 protons in a polyisobutylene sample. It has been shown that the main pathway for magnetization exchange occurs only within the monomer unit of a single chain [83]. That is why we assume that intermolecular spin-exchange involving the shortest interatomic ^{1}H–^{1}H distance within one molecule (see Fig. 13) is the dominant process during the initial step of polarization transfer.

Dependences of cross-peak intensities on mixing time as depicted in Fig. 12A clearly reflect a substantial difference in the spin-exchange rate between two nonequivalent α-protons and between α-protons and NH_3^+ groups. There is a remarkable decrease in intensity of the signal correlating nonequivalent α-protons during later stages of polarization transfer, which clearly indicates a substantially smaller spin-exchange rate constant driving polarization transfer between αH and NH_3^+ protons. To determine the spin-exchange coefficient exactly and to avoid the decrease of cross-peak signal intensity, polarization transfer between nonequivalent α-protons was analyzed separately (see Fig. 12B). On the basis of the known

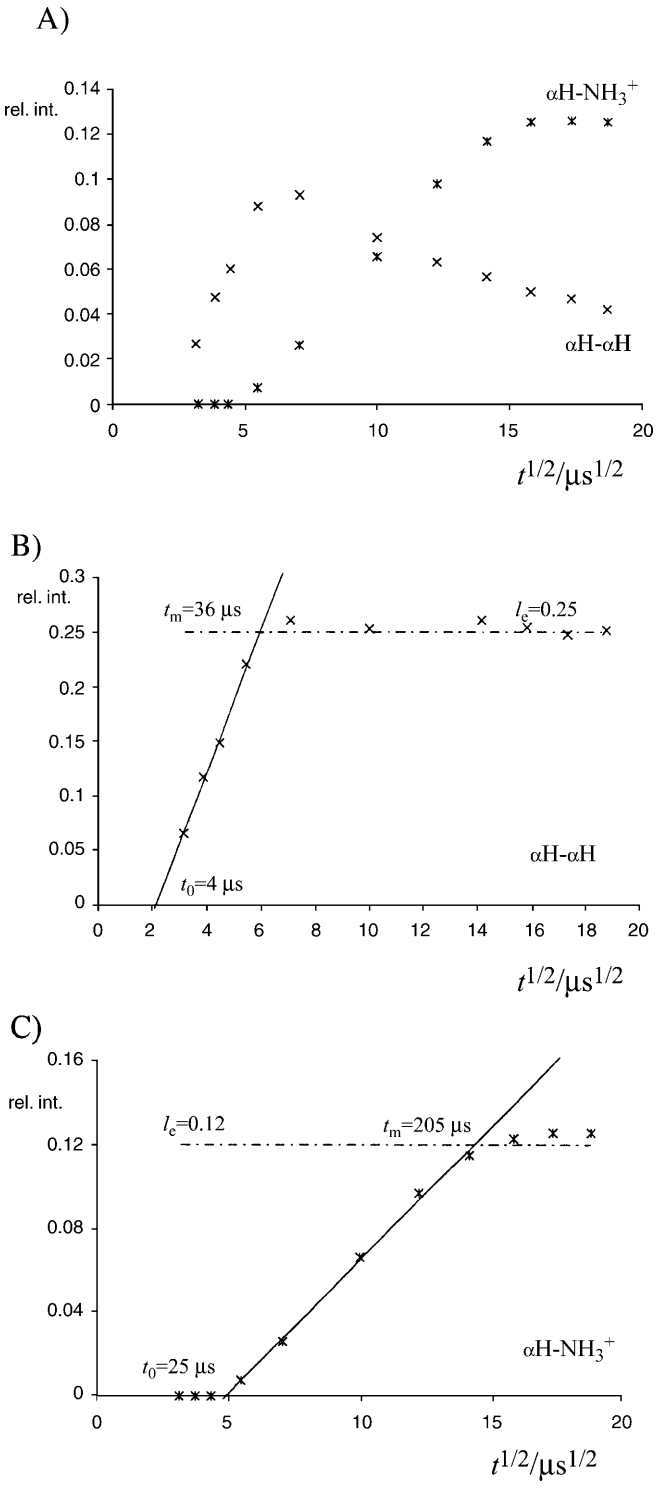

Fig. 12. (A) Evolution of the correlation signal intensity as a function of $\sqrt{t_m}$; (B) Experimental spin-exchange built-up curve and simulation of its linear part for polarization transfer between nonequivalent α-protons; (C) Experimental spin-exchange built-up curves and simulation of the linear parts for polarization transfer between nonequivalent α-H and NH_3^+ protons in glycine

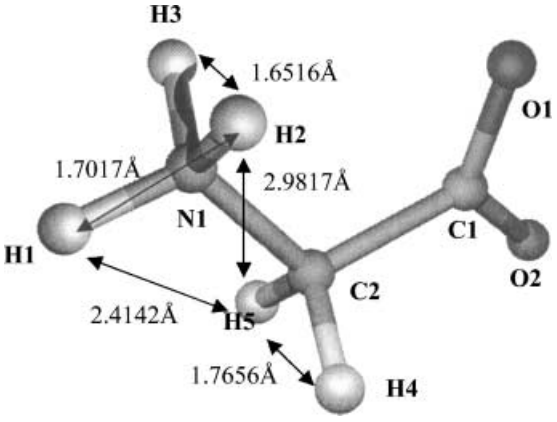

Fig. 13. Geometry of glycine molecules in the crystal unit cell obtained from neutron diffraction data [84]

interatomic distance between α-protons (1.77 nm) [84], and mixing time ($t_m = 32\,\mu s$), which is necessary to achieve the equilibrium intensity of the corresponding cross-peak, the spin-exchange constant $D = 0.77\,nm^2\,ms^{-1}$ was derived. The calculated spin-exchange coefficient corresponds to the values generally reported in literature for rigid organic solids, $D = 0.7–0.8\,nm^2\,ms^{-1}$.

In the next step, we analyzed the spin-exchange process between αH and NH_3^+ protons. Generally it is accepted that in a system with uniform internal mobility, the determined spin-exchange constant is the same for all spin-pairs. Thus, assuming that the motion of the system is homogeneous (*i.e.* applying $D = 0.77\,nm^2\,ms^{-1}$), the analysis of spin-exchange processes between α-H and NH_3^+ protons should reveal interatomic distances corresponding to *ca.* 0.24–0.25 nm (neutron diffraction data [84]).

The long delay at the beginning of the polarization transfer process during which no off-diagonal cross-peak correlating αH and NH_3^+ protons evolves (see Fig. 12C) probably corresponds to back polarization exchange within each ^1H moiety. A similar, but not quite the same phenomenon has been observed by *de Groot et al.* [85] in heteronuclear polarization transfer experiment probing $^1H–^{13}C$ interatomic distances in tyrosine. Due to this fact we believe that this delay-time can be substracted from the experimentally determined equilibrium mixing times ($t_m = 205\,\mu s$). However, even with this correction and using equilibrium mixing times $t_m = 181\,\mu s$ the calculated distance between NH_3^+ and αH is very large ($r = 0.43$ nm). This deviation cannot be simply explained by relayed coherence transfer, because assuming the largest coherence pathway (αH-1 $\rightarrow$ αH-2 $\rightarrow$ NH-1 $\rightarrow$ NH-2) the time which would be necessary to achieve equilibrium intensity is only $t_m = 32 + 58 + 29 = 119\,\mu s$. From this, it is clear that the rotation of the NH_3^+ group predominantly affects the rate of spin-exchange. The local molecular motion averages dipolar interactions and consequently the corresponding spin-exchange rate constant is reduced. The corresponding spin-exchange rate constant driving polarization transfer between NH_3^+ and αH is scaled down by a factor of approximately 3.5 ($D^* = 0.24\,nm^2\,ms^{-1}$).

Although the difference in internal motions cannot be observed by standard ^1H NMR experiments, analysis of ^2H NMR line-shapes of selectively deuterium

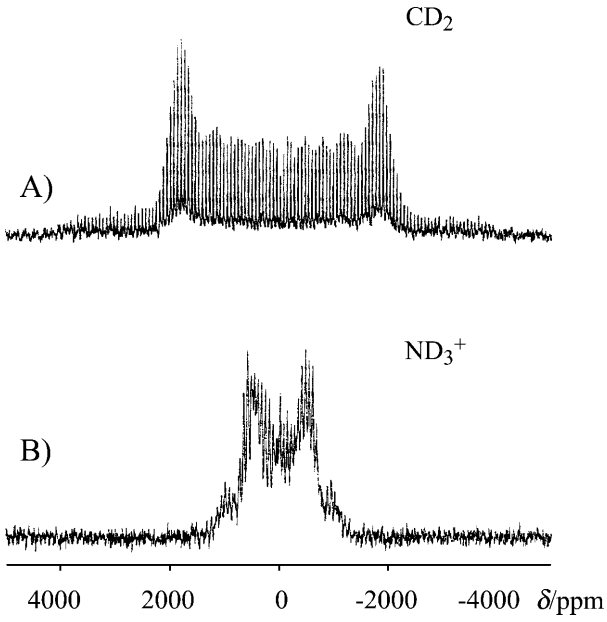

Fig. 14. ^{2}H MAS spectra of selectively deuterated samples: (A) $NH_3^+CD_2COO^-$, (B) $ND_3^+CH_2COO^-$

labeled samples (see Fig. 14) directly proved a difference in the local mobilities of CD_2 and ND_3^+ moieties. The ^{2}H quadrupole splitting QCC is approximately three times smaller for the amino group compared with the methylene one, which nicely correlates to the observed decrease of the spin-exchange constant: $D^*/D \cong QCC(ND_3^+)/QCC(CD_2) \cong 1/3.5$.

Hence, the relative spin-exchange rate constants can be evaluated on the basis of the knowledge of the ^{2}H line-shape of specific sites.

Determination of ^{1}H–^{1}H Interatomic Distance Through ^{13}C–^{13}C Correlation

The simple ^{1}H–^{1}H correlation experiment just discussed is sufficient only for small molecular systems. For larger macromolecules, spectral resolution has to be increased, *e.g.* by application of 3D ^{1}H–^{1}H–^{13}C techniques [30] as mentioned above or 2D ^{13}C–^{13}C correlation mediated by ^{1}H–^{1}H spin-exchange [55, 86] (see Fig. 15). Although the later experiment looks very promising as it should allow to determine short ^{1}H–^{1}H interatomic distances (see Fig. 16A), it has been used so far only to assign ^{15}N resonance in uniformly labeled biological solids [87], to study the degree of mixing of principal and secondary phase of $Zn(O_3PC_2H_4COOH)0 \cdot 5C_6H_5NH_2$ through ^{31}P–^{31}P correlation [88], or to evaluate the degree of phase separation and domain size in selectively labeled polymer blends [86]. This means that predominantly distances in the nonometer length scale have been probed. The impossibility to determine shorter distances by this experiment follows from the application of a cross-polarization (CP) step for coherence transfer. It is known that ^{1}H–^{1}H spin-exchange occurs not only for z magnetization but also for spin-locked transverse ^{1}H magnetization, for instance under *Hartman-Hahn* CP [89, 90]. Under sample rotation, the locking field scales the dipolar coupling by a factor 1/2, which causes

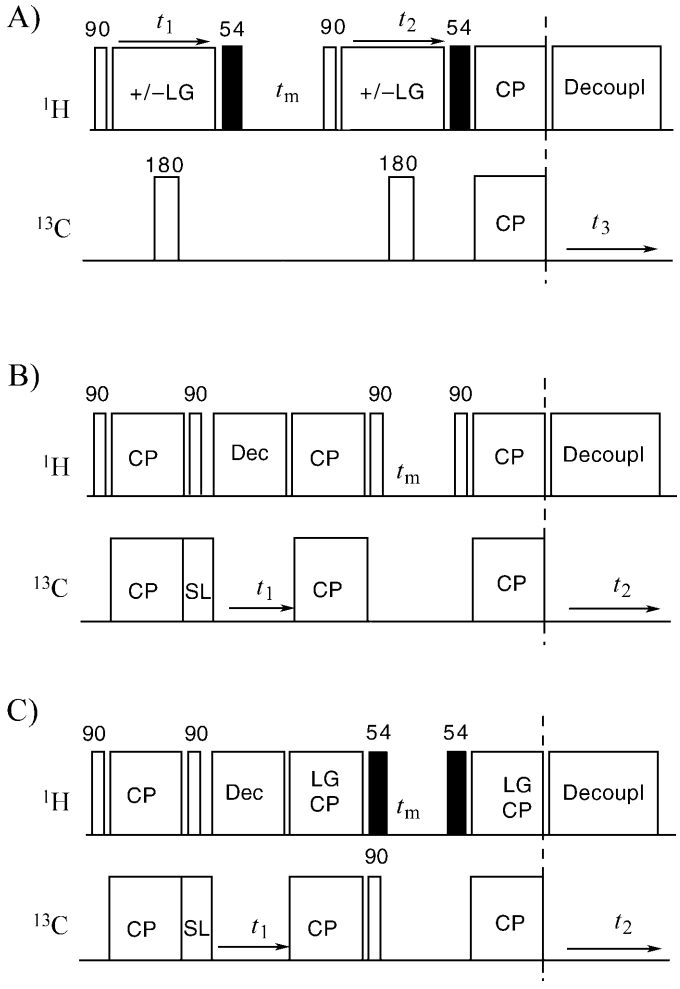

Fig. 15. (A) Pulse scheme of 3D spin-exchange experiment with *Lee-Goldburg* decoupling during both indirect ^{1}H detection period [30]; (B) 2D ^{13}C–^{13}C correlation experiment mediated by ^{1}H–^{1}H spin-exchange [54]; (C) Modification of B by *Lee-Goldburg*-CP and magic angle pulses (SL – spin lock, CP – cross-polarization, LG – *Lee-Goldburg*, Dec. – heteronuclear decoupling)

slowing down of the spin-exchange process by one half during CP as compared with the standard spin-exchange rate taking part in z direction. However, the spin exchange is not completely quenched. As the spin-exchange process in rigid solids is very fast (several tens of microseconds is sufficient to achieve equilibrium), a high degree of equilibration is achieved even at very short cross-polarization times without any mixing time.

In the case of this 2D ^{13}C–^{13}C correlation experiment, the relevant CP steps complicating the evolution of cross-peak intensity are the second and the third one. As the result of this undesired coherence transfer one can clearly see cross-peaks in the 2D spectrum of uniformly ^{13}C enriched alanine which was acquired with zero mixing time and very short cross-polarization periods (see Fig. 16B). Due to these artificial signals, the experimentally determined dependence of cross-peak intensity on mixing time is not suitable for accurate analysis (see Fig. 17A).

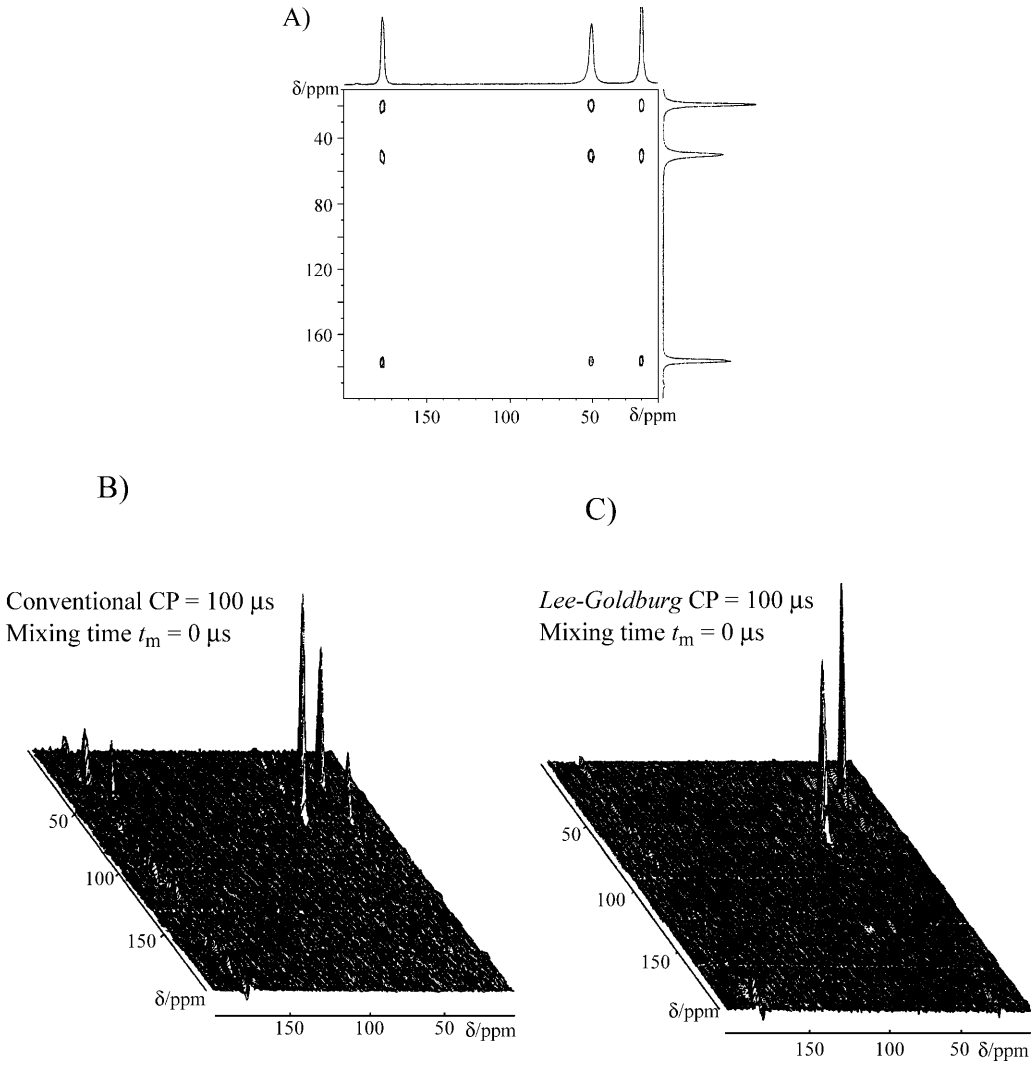

Fig. 16. 2D ^{13}C–^{13}C correlation spectra of U–^{13}C, ^{15}N Alanine measured at: (A) 100 ms cross-polarization (CP) time and 1 ms mixing time; (B) 100 ms CP time and zero mixing time; (C) 100 ms *Lee-Goldburg* CP time and zero mixing time

Spin-exchange during CP has to be suppressed and the artifacts have to be removed to be able to analyze the evolution of cross-peak intensity. A very promising tool to suppress ^{1}H–^{1}H dipolar interactions is provided by *Lee-Goldburg* irradiation [23]. Applying this technique, for instance during acquisition of the ^{13}C resonance, the ^{1}H–^{1}H spin-diffusion is suppressed and the resulting spectrum contains multiplets reflecting the number of *J*-coupled protons. It has been shown that the *Lee-Goldburg* irradiation can also be applied during the cross-polarization transfer step [85]. Observation of intense transient dipolar oscillation in the case of *Lee-Goldburg* CP confirms the suppression of ^{1}H–^{1}H spin-exchange. Recently, it has been shown that an analysis of this dipolar oscillation reflecting dipolar coupling between directly bonded ^{1}H–^{13}C spin pairs can be used to obtain accurate ^{1}H–^{13}C interatomic distances [85]. In the case of conventional on-resonance CP

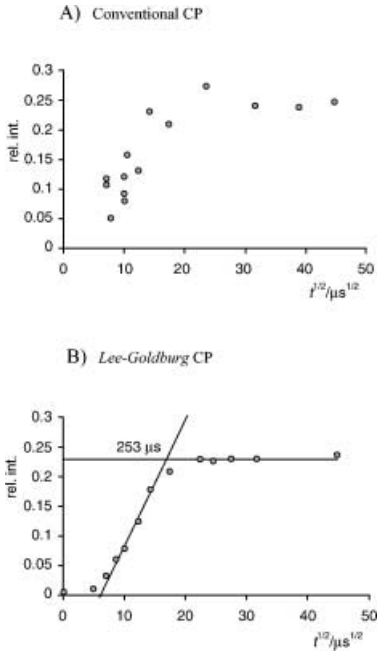

Fig. 17. Spin-exchange built-up curves obtained by application of conventional experiment (A) and by modified pulse sequence with *Lee-Goldburg*-CP (B)

such dipolar oscillation is almost completely destroyed as a result of fast ^{1}H–^{1}H spin exchange involving many ^{1}H spins. By application of *Lee-Goldburg* CP for the second and the third polarization transfer in the 2D ^{13}C–^{13}C correlation pulse sequence the unwanted spin-exchange was suppressed. The original 90° ^{1}H pulses (exactly, the third and the fourth one) have been replaced by magic angle pulses.

In the resulting 2D spectrum measured with *Lee-Goldburg* CP and without any mixing period the unwanted artificial cross-peaks are completely canceled. In addition, signal intensities of diagonal signals are not distorted when applying *LG*-CP. From the obtained dependence of cross-peak intensity on mixing time (see Fig. 17B), which is now suitable for accurate analysis, one can determine the desired information about ^{1}H–^{1}H interatomic distance with high accuracy according to the procedures mentioned in the previous sections.

Conclusion

In this contribution, we briefly summarized basic experimental techniques leading to averaging of ^{1}H–^{1}H dipolar interaction and allowing thus to obtain highly resolved ^{1}H NMR spectra of organic solids. Spin-diffusion experiments providing an interesting probe to geometry and structure of several systems were introduced and analysis of resulting data was discussed. The power of theses 2D spin-exchange experiments was demonstrated on several complex systems. At first, the degree of mixing of polymer components was evaluated for the semicrystalline blend *PC-PEO* and a further detailed analysis of complex spin-diffusion process led to an estimate of the size of polymer domains in the diblock copolymer *PE-PEO*. The same approach was used to investigate clustering of surface hydroxyls

on a silica network and to determine the average size of various hydroxyl clusters. It was also shown that the same experiments and procedures can be used to determine very short interatomic $^{1}H–^{1}H$ distances, although the variation in internal motions has to be carefully investigated and described. Finally we discussed the possibility of the application of 2D $^{13}C–^{13}C$ correlation experiments exploiting $^{1}H–^{1}H$ spin exchange to determine structural constrains.

Experimental

NMR Spectroscopy

NMR spectra were measured using a Bruker DSX 200 NMR spectrometer (Karlsruhe, Germany) in 4 and 7 mm ZrO_2 rotors at frequencies 50.33 and 200.14 MHz (^{13}C and ^{1}H, respectively). For acquisition of ^{1}H MAS NMR spectra, the spinning frequency was 0–16 kHz and the strength of the B_1 field 62.5 kHz ($\pi/2$ pulse 4 μs). 1D CRAMPS spectra at slow MAS (2 kHz) were acquired using the BR-24 pulse sequence [18]. A 2D spin-exchange experiment proposed by *Caravatti et al.* [63] was used to observe $^{1}H–^{1}H$ correlation. In direct and indirect detection periods the BR24 pulse sequence was used. Spin-diffusion mixing times varied from 0.1 to 40 ms. The intensity of the B_1 field was 140 kHz ($\pi/2$ pulse 1.8 μs) and small and large windows were 1.0 and 3.8 μs, respectively. The ^{1}H scale was calibrated with glycine as an external standard (low-field NH_3^+ signal at 8.0 ppm and the high field α-H signal at 2.8 ppm). 2D $^{13}C–^{13}C$ correlation spectra were obtained with a pulse sequence proposed by *de Groot et al.* and *Spiess et al.* [55, 86] at 11 kHz. The strength of the B_1 field applied for the *Lee-Goldburg* cross-polarization was 83 kHz, with ^{1}H resonance offset 64.6 kHz.

Materials

The *PC-PEO* blend was prepared from commercial-grade Bisphenol A polycarbonate SINVET 251 (ENI, Italy) with a weight-average molecular weight (M_w) of 24000 and a number-average molecular weight (M_n) of 9600, and from *PEO* ($M_w = 6 \times 10^5$) produced by BDH Chemicals, Ltd. (UK). The sample of *PC-PEO* blend was obtained by dropwise precipitation from a $CHCl_3$ solution (2% w/w) into pentane, slow evaporation of the solvents at room temperature and subsequent heating in a vacuum oven at 85°C for 1 h.

The block-copolymers *PE-PEO* $M_n(PE) = 4700$, $M_n(PEO) = 4700$ was used without any purification as purchased from Polymer Source, Inc.

Siloxane materials *TE* and *TE-DM* were prepared by acid-catalyzed sol-gel polycondensation of mixtures: tetraehoxysilane (*TEOS*)/C_2H_5OH/H_2O/HCl and tetraethoxysilane/dimethyldiethoxysilane (*DMDEOS*)/C_2H_5OH/H_2O/HCl in mole ratios 1/4.50/3/0.03 and 0.75/0.25/4.50/3/0.03, respectively. *TEOS* and *DMDEOS* were purchased from Wacker-Chemie GmbH., Germany. HCl was added to a mixture of alkoxysilanes with ethanol. The resulting mixture (*ca.* 10 g) was stirred for 30 min and subsequently poured onto a *Petri* dish (5.5 cm in diameter). Polycondensation then took place under laboratory conditions. After a year, the products were finely powdered and placed into an air-conditioned box (relative humidity – RH = 55%, $t = 25$°C) for one month. Partially deuterated samples were obtained by simple exchange with deuterium oxide at laboratory temperature and pressure in a close vessel containing a dish with D_2O. After the deuteration procedure the samples were not subsequently dried. Deuterium exchange periods were 24 h.

Glycine and U–^{15}N,^{13}C Alanine were used as purchased from Aldrich.

Acknowledgement

The authors thank the Grant Agency of the Academy of Sciences of the Czech Republic (grant IAB4050203, IAA4050208 and grant AVOZ4050913) for financial support.

References

[1] Mehring M (1983) In: Principles of high resolution NMR in solids, Springer, Berlin
[2] Schmidt-Rohr K, Spiess HW (1994) In: Multidimensional solid-state NMR and polymers, Academic Press, London
[3] Lowe IJ (1959) Phys Rev Lett **2**: 285
[4] Marciq MM, Waugh JS (1979) J Chem Phys **70**: 3300
[5] Samoson A, Tuherm T (1999) In: Proceedings, the 1-st alpine conference on solid-state NMR, Chamonix-Mont Blanc, France
[6] Bjorholm T, Jakobsen HJ (1989) J Magn Reson **84**: 204
[7] Bielecki A, Burum DP (1995) J Magn Reson A **116**: 215
[8] Aguilar-Parrila F, Wehrle B, Braunling H, Limbach HH (1990) J Magn Reson **87**: 592
[9] Brus J (2000) Solid State Nucl Magn Reson **16**: 151
[10] Waugh JS, Huber LM, Haeberlen U (1968) Phys Rev Lett **20**: 453
[11] Haeberlen U, Waugh JS (1968) Phys Rev Lett **20**: 180
[12] Farrar TC (1990) Concepts Magn Reson **2**: 55
[13] Smith SA, Palke WE, Gerig JT (1993) Concepts Magn Reson **5**: 151
[14] Gerstein BC, Pembleton RG, Wilson RC, Ryan LM (1977) J Magn Reson **66**: 361
[15] Maciel GE, Bronnimann CE, Hawkins B (1990) Adv Magn Reson **14**: 125
[16] Dec SF, Bronnimann CE, Wind RA, Maciel GE (1989) J Magn Reson **82**: 454
[17] Rhim WK, Elleman DD, Vaughan RW (1973) J Chem Phys **59**: 3740
[18] Burum DP, Rhim WK (1979) J Chem Phys **71**: 944
[19] Bronnimann CE, Hawkins BL, Zhang M, Maciel GE (1988) Anal Chem **60**: 1743
[20] Hafner S, Spiess HW (1996) J Magn Reson A **121**: 160
[21] Demco DE, Hafner S, Spiess HW (1995) J Magn Reson **116**: 36
[22] Hafner S, Spiess HW (1997) Solid State Nucl Magn Reson **8**: 17
[23] Lee M, Goldburg WI (1965) Phys Rev A **140**: 1261
[24] Bielecki A, Kolbert AC, Levitt MH (1989) Chem Phys Lett **155**: 341
[25] Bielecki A, Kolbert AC, de Groot HJM, Griffin RG, Levitt MH (1990) Adv Magn Reson **14**: 111
[26] Lesage A, Steuernagel S, Emsley L (1998) J Am Chem Soc **120**: 7095
[27] Lesage A, Duma L, Sakellariou D, Emsley L (2001) J Am Chem Soc **123**: 5747
[28] Vinaogradov E, Madhu PK, Vega S (1999) Chem Phys Lett **314**: 443
[29] Ramamoorthy A, Gierasch LM, Opella SJ (1996) J Mag Reson Ser B **111**: 81
[30] Sakellariou D, Lesage A, Emsley L (2001) J Am Chem Soc **123**: 5604
[31] Vinogradov E, Madhu PK, Vega S (2002) Chem Phys Lett **354**: 193
[32] Levitt MH, Kolbert AC, Bielecki A, Ruben DJ (1993) Solid State NMR **2**: 151
[33] Bloembergen N (1949) Physica **15**: 386
[34] Zhang S, Meier BH, Ernst RR (1992) Phys Rev Lett **69**: 2149
[35] Abragam A (1961) In: The Principles of Nuclear Magnetism, Oxford University Press, London
[36] Clauss J, Schmidt-Rohr K, Spiess HW (1993) Acta Polym **44**: 1
[37] Cheung TTP (1999) J Phys Chem B **103**: 9423
[38] Demco DE, Johanson A, Tegenfeldt J (1995) Solid State Nucl Magn Reson **4**: 13
[39] VanderHart DL, McFadden GB (1996) Solid State Nucl Magn Reson **7**: 45
[40] Campbell GC, Vander Hart DL (1992) J Magn Reson **96**: 69
[41] Mellinger F, Wilhelm M, Spiess HW (1999) Macromolecules **32**: 4686
[42] Holstein P, Monti GA, Harris RK (1999) Phys Chem Chem Phys **1**: 3549
[43] Cheung TTP (1981) Phys Rev B **23**: 1404
[44] Cheung TTP, Gerstein BC (1981) J Appl Phys **52**: 5517
[45] Chin YH, Kaplan S (1994) Magn Res in Chem **32**: S53
[46] Weigand F, Demco DE, Blümich B, Spiess HW (1996) J Magn Reson Ser A **120**: 190
[47] Hu WG, Schmidt-Rohr K (2000) Polymer **41**: 2979

[48] Brus J, Dybal J, Schmidt P, Kratochvíl P, Baldrian J (2000) Macromolecules **33**: 6448
[49] Spiegel S, Schmidt-Rohr K, Böffel C, Spiess HW (1993) Polymer **34**: 4566
[50] Lehmann SA, Meltzer AD, Spiess HW (1998) J Polym Sci, Part B, Polym Phys **36**: 693
[51] Clauss J, Schmidt-Rohr K, Adam A, Boeffel C, Spiess HW (1992) Macromolecules **25**: 5208
[52] Cheung MK, Wang J, Zheng S, Mi Y (2000) Polymer **41**: 1469
[53] Brus J, Dybal J, Sysel P, Hobzová R (2002) Macromolecules **35**: 1253
[54] Clayden NJ, Nijs CL, Eeckhaut GJ (1997) Polymer **38**: 1011
[55] Wilhelm M, Feng H, Tracht U, Spiess HW (1998) J Magn Reson **134**: 255
[56] Mirau PA, Shu Yang (2002) Chem Mater **14**: 249
[57] Goldman M, Shen L (1996) Phys Rev **144**: 321
[58] VanderHart DL, Feng Y, Han CC, Weiss RA (2000) Macromolecules **33**: 2206
[59] Beshah K, Molnar LK (2000) Macromolecules **33**: 1036
[60] Schmidt-Rohr K, Clauss J, Blumich B, Spiess HW (1990) Magn Res in Chem **28**: 3
[61] Caravatti P, Lewitt MH, Ernst RR (1986) J Magn Reson **68**: 323
[62] Caravatti P, Neuenschwander P, Ernst RR (1986) Macromolecules **19**: 1889
[63] Caravatti P, Neuenschwander P, Ernst RR (1985) Macromolecules **18**: 119
[64] Nouwen J, Adriaensens P, Gelan J, Verreyt G, Yang Z, Geise HJ (1994) Macromol Chem Phys **195**: 2469
[65] Belfiore LA, Graham H, Veda E, Wang Y (1992) Polym Int **28**: 81
[66] Schaller T, Sebald A (1995) Solid State NMR **5**: 89
[67] Babonneau F, Gualandris V, Maquet J, Massiot D, Janicke MT, Chmelka BF (2000) J Sol-Gel Sci & Techn **19**: 113
[68] Mirau PA, Heffner SA, Schilling M (1999) Chem Phys Lett **313**: 139
[69] Heffner SA, Mirau PA (1994) Macromolecules **27**: 7283
[70] Huster D, Yao X, Hong M (2002) J Am Chem Soc **124**: 874
[71] Brus J, Dybal J (2002) Macromolecules (in press)
[72] Chuang IS, Maciel GE (1997) J Phys Chem B **101**: 3052
[73] Kinney DR, Chuang IS, Maciel GE (1993) J Am Chem Soc **115**: 6786
[74] Changhua CL, Maciel GE (1996) J Am Chem Soc **118**: 5103
[75] Chuang IS, Kinney DR, Maciel GE (1996) J Am Chem Soc **118**: 8695
[76] Assink RA (1978) Macromolecules **11**: 1233
[77] Lesage A, Emsley L (2001) J Magn Reson **148**: 449
[78] Sakellariou D, Lesage A, Hodgkinson P, Emsley L (2000) Chem Phys Lett **319**: 253
[79] Brus J, Petrickova H, Dybal J (2002) Solid State NMR (submitted)
[80] Kimura H, Nakamura K, Eguchi A, Sugisawa H, Deguchi K, Ebisawa K, Suzuki E, Shoji A (1998) J Mol Struct **447**: 247
[81] Naito A, Root A, McDowell CA (1991) J Phys Chem **95**: 3578
[82] Jackson P, Harris RK (1995) J Chem Soc Faraday Trans **91**: 805
[83] Wang X, White JL (2002) Macromolecules **35**: 3795
[84] Power LF, Turner KE, Moore FH (1976) Acta Crystallogr **B32**: 11
[85] van Rossum BJ, de Groot CP, Ladizhansky V, Vega S, de Groot HJM (2000) J Am Chem Soc **122**: 3465
[86] Mulder FM, Heinen W, van Duin M, Lugtenburg J, de Groot HJM (1998) J Am Chem Soc **120**: 12891
[87] Wei Yufeng, Ramamoorthy A (2001) Chem Phys Lett **342**: 312
[88] Massiot D, Alonso B, Fayon F, Fredoueil F, Bujoli B (2001) Solid State Sci **3**: 11
[89] Hartmann SR, Hahn EL (1962) Phys Rev **128**: 2042
[90] Pines A, Gibby MG, Waugh JS (1973) J Chem Phys **59**: 569